Deswelling Dynamics of Chemically-Active Polyelectrolyte Gels *

Bindi M. Nagda[1], Jian Du[1], Owen L. Lewis[2], Aaron L. Fogelson[3]

[1] Florida Institute of Technology, Melbourne FL 32901, USA
jdu@fit.edu
[2] University of New Mexico, Albuquerque NM 87106, USA
[3] University of Utah, Salt Lake City UT 84112, USA

Abstract. Ion-induced volume phase transitions in polyelectrolyte gels play an important role in physiological processes such as mucus storage and secretion in the gut, nerve excitation, and DNA packaging. Experiments have shown that changes in ionic composition can trigger rapid swelling and deswelling of these gels. Based on a previously developed computational model, we carry out 2D simulations of gel deswelling within an ionic bath. The dynamics of the volume phase transition are governed by the balance of chemical and mechanical forces on components of the gel. Our simulation results highlight the close connections between the patterns of deswelling, the ionic composition, and the relative magnitude of particle-particle interaction energies.

Keywords: Polyelectrolyte Gel · Deswelling · Multiphase Model · Simulation

1 Introduction

Polyelectrolyte gels are mixtures of a polymer network, a solvent and ions that are either bound to the network or dissolved in the solvent. They are prevalent in living systems, from polynucleotides like DNA molecules [1] to the glycoproteins that form a protective gastric mucus layer [2]. Experiments have shown that monovalent/divalent ion exchange between the polymer and the solvent plays a major role in inducing a volume transition in polyelectrolyte gels [3]. These volume transitions are important role in physiology, a prime example is their role in maintenance of the gastric mucus layer. Gastric mucus is a highly hydrated network consisting mainly of water mixed with mucin polymers and other electrolytes [2]. Goblet cells in the gut produce mucin and densely pack it in lipid vesicles. Inside these vesicles, high concentrations of divalent calcium ions keep the mucin network in a dehydrated state by crosslinking negatively charged groups between two polymer strands. A stimuli such as change in ionic composition can triggerff the release of these mucins into the extracellular environment, whereby they swell explosively on a timescale of milliseconds [2].

* Supported by NIH research grant 1R01GM131408

ICCS Camera Ready Version 2023
To cite this paper please use the final published version:
DOI: 10.1007/978-3-031-36030-5_27

Pioneering work on volume transitions investigated the thermodynamic equilibrium of the gel and its dependence on parameters such as pH and temperature [4]. Later investigations of non-equilibrium transient states of swelling were based on simplifications such as a reduced model for the fluid flow, or low polymer volume fractions [5]. Recent models have addressed gel dynamics and included effects of electrochemical potentials [6]. These studies are based on the classical Flory-Huggins mixture theory [7], and do not generalize the mixing energy to account for ion/polymer chemical reactions or the network's affinity for binding with divalent cations. To address this gap, a multiphase model for polyelectrolyte gel swelling was developed with the formulation based on chemical potentials [8]. More recently, the model was rederived and extended to use force densities (i.e. potential gradients) rather than chemical potentials to reveal the underlying causes of the swelling behavior [9]. A computational method for simulating gel swelling dynamics in 2D was proposed in [10], based on a novel algorithm for evolving the dissolved ion concentrations and the electric potential originally presented in [11].

In this paper, we extend the computational investigation towards analyzing deswelling dynamics in 2D by characterizing the contributions of the forces acting on the network and solvent due to short-range interactions. In Section 2, we present the model equations that govern the dynamics of a two-phase gel. In Section 3, describe simulation results from two sets of computational experiments. We see that in one parameter regime, exposure of a low density gel to a bath of divalent calcium leads to a deswelling or condensation of the gel, with the speed and degree of deswelling controlled by the bath concentration. However, in another regime (defined by the relative size of particle-particle interaction energies), exposure to a divalent bath can lead to a qualitatively distinct form of collapse where-in a high density "ring" of network forms at the periphery of the gel sample. Finally in Section 4, we present a conclusion of our findings and highlight the key points from our study.

2 Model

Our model incorporates a two-fluid description of the solvent phase (s) and the network phase (n) of the gel, as well as the evolution of the dissolved and bound ion concentrations, included through binding and unbinding reactions between cations and the negatively charged network. It accounts for a number of mechanical forces (viscous, drag, pressure) and "chemical forces" (entropic, electric, short-range interactions), which depend on the spatial distribution of the network and solvent phases, the ionic species, and their respective velocities. Full details about the derivation can be found in [9]. The model equations are a coupled system of nonlinear PDEs along with two constraints – incompressibility and electroneutrality of the mixture at all points in space and time.

We denote the volume fraction of the network and solvent as θ_{n} and θ_{s}, respectively. The dynamics of the two volume fractions are governed by the

ICCS Camera Ready Version 2023
To cite this paper please use the final published version:
DOI: 10.1007/978-3-031-36030-5_27

advection equations

$$\frac{\partial}{\partial t}\theta_{\mathrm{n}} + \nabla\cdot(\theta_{\mathrm{n}}\mathbf{u}_{\mathrm{n}}) = 0, \qquad \frac{\partial}{\partial t}\theta_{\mathrm{s}} + \nabla\cdot(\theta_{\mathrm{s}}\mathbf{u}_{\mathrm{s}}) = 0. \tag{1}$$

Here $\mathbf{u}_{\mathrm{n}}$ and $\mathbf{u}_{\mathrm{s}}$ are the velocity of the network and solvent, respectively. These equations along with the identity $\theta_{\mathrm{n}}(\boldsymbol{x},t)+\theta_{\mathrm{s}}(\boldsymbol{x},t) = 1$ yield the volume-averaged incompressibility condition

$$\nabla\cdot(\theta_{\mathrm{n}}\mathbf{u}_{\mathrm{n}} + \theta_{\mathrm{s}}\mathbf{u}_{\mathrm{s}}) = 0. \tag{2}$$

Dissolved sodium and calcium ions can bind to and unbind from negatively charged sites on the network according to the following reactions. Here M refers to a monomer that carries one negative charge. $k_{\mathrm{j}}^{\mathrm{on}}$ and $k_{\mathrm{j}}^{\mathrm{off}}$ are the binding and unbinding rates for ion j, respectively.

$$\mathrm{M}^- + \mathrm{Na}^+ \underset{k_{\mathrm{Na}}^{\mathrm{off}}}{\overset{k_{\mathrm{Na}}^{\mathrm{on}}}{\rightleftharpoons}} \mathrm{MNa}, \quad \mathrm{M}^- + \mathrm{Ca}^{2+} \underset{k_{\mathrm{Ca}}^{\mathrm{off}}}{\overset{k_{\mathrm{Ca}}^{\mathrm{on}}}{\rightleftharpoons}} \mathrm{MCa}^+, \quad \mathrm{M}^- + \mathrm{MCa}^+ \underset{2k_{\mathrm{Ca}}^{\mathrm{off}}}{\overset{\frac{1}{2}k_{\mathrm{Ca}}^{\mathrm{on}}}{\rightleftharpoons}} \mathrm{M_2Ca}. \tag{3}$$

The concentrations (per unit solvent volume) of dissolved sodium, calcium, and chloride ions are denoted C_{Na}, C_{Ca}, and C_{Cl}, respectively. They are governed by the Nernst-Planck equations (4)-(6). The ions move by advection at the solvent velocity, diffusion, and electromigration, and participate in binding/unbinding reactions with the network. Ψ is the electrical potential scaled by $\frac{q}{k_B T}$, where q is the fundamental charge, k_B is the Boltzmann constant, and T is the temperature. The value of Ψ is determined by the electroneutrality constraint, Eq. (10). D_{Na}, D_{Ca}, and D_{Cl} are the ion diffusion coefficients.

$$\frac{\partial C_{\mathrm{Na}}}{\partial t} + \mathbf{u}_{\mathrm{s}}\cdot\nabla C_{\mathrm{Na}} = \frac{1}{\theta_{\mathrm{s}}}\nabla\cdot\Big(\theta_{\mathrm{s}} D_{\mathrm{Na}}\left(\nabla C_{\mathrm{Na}} + C_{\mathrm{Na}}\nabla\Psi\right)\Big) - k_{\mathrm{Na}}^{\mathrm{on}} m C_{\mathrm{Na}} + k_{\mathrm{Na}}^{\mathrm{off}} B_{\mathrm{MNa}}\theta_{\mathrm{s}}, \tag{4}$$

$$\frac{\partial C_{\mathrm{Ca}}}{\partial t} + \mathbf{u}_{\mathrm{s}}\cdot\nabla C_{\mathrm{Ca}} = \frac{1}{\theta_{\mathrm{s}}}\nabla\cdot\Big(\theta_{\mathrm{s}} D_{\mathrm{Ca}}\left(\nabla C_{\mathrm{Na}} + 2C_{\mathrm{Ca}}\nabla\Psi\right)\Big) - k_{\mathrm{Ca}}^{\mathrm{on}} m C_{\mathrm{Ca}} + k_{\mathrm{Ca}}^{\mathrm{off}} B_{\mathrm{MCa}}\theta_{\mathrm{s}}, \tag{5}$$

$$\frac{\partial C_{\mathrm{Cl}}}{\partial t} + \mathbf{u}_{\mathrm{s}}\cdot\nabla C_{\mathrm{Cl}} = \frac{1}{\theta_{\mathrm{s}}}\nabla\cdot\Big(\theta_{\mathrm{s}} D_{\mathrm{Cl}}\left(\nabla C_{\mathrm{Cl}} - C_{\mathrm{Cl}}\nabla\Psi\right)\Big), \tag{6}$$

The concentrations (per total volume) of ions bound to the network are denoted B_{MNa}, B_{MCa} and $B_{\mathrm{M_2Ca}}$ for sodium bound to monomer, calcium bound to a single monomer, and calcium bound to two monomers, respectively. They are affected by the ions' advection at the network velocity and their participation in binding/unbinding reactions.

$$\frac{\partial B_{\mathrm{MNa}}}{\partial t} + \nabla\cdot(\mathbf{u}_{\mathrm{n}} B_{\mathrm{MNa}}) = k_{\mathrm{Na}}^{\mathrm{on}} m C_{\mathrm{Na}}\theta_{\mathrm{s}} - k_{\mathrm{Na}}^{\mathrm{off}} B_{\mathrm{MNa}}{\theta_{\mathrm{s}}}^2, \tag{7}$$

$$\frac{\partial B_{\mathrm{MCa}}}{\partial t} + \nabla\cdot(\mathbf{u}_{\mathrm{n}} B_{\mathrm{MCa}}) = k_{\mathrm{Ca}}^{\mathrm{on}} m C_{\mathrm{Ca}}\theta_{\mathrm{s}} - k_{\mathrm{Ca}}^{\mathrm{off}} B_{\mathrm{MCa}}{\theta_{\mathrm{s}}}^2 + 2k_{\mathrm{Ca}}^{\mathrm{off}} B_{\mathrm{M_2Ca}} - \frac{1}{2}k_{\mathrm{Ca}}^{\mathrm{on}} m B_{\mathrm{MCa}}, \tag{8}$$

ICCS Camera Ready Version 2023
To cite this paper please use the final published version:
DOI: 10.1007/978-3-031-36030-5_27

$$\frac{\partial B_{\mathrm{M_2Ca}}}{\partial t} + \nabla \cdot (\mathbf{u}_{\mathrm{n}} B_{\mathrm{M_2Ca}}) = -2k_{\mathrm{Ca}}^{\mathrm{off}} B_{\mathrm{M_2Ca}} + \frac{1}{2} k_{\mathrm{Ca}}^{\mathrm{on}} m B_{\mathrm{MCa}}, \tag{9}$$

In Eqs. (4)-(9), m is the concentration of unoccupied binding sites on the network, which is calculated as $m = n^{\mathrm{tot}}\theta_{\mathrm{n}} - B_{\mathrm{MNa}} - B_{\mathrm{MCa}} - 2B_{\mathrm{M_2Ca}}$ (n^{tot} is defined below.). The electroneutrality condition is that the concentration of charge is zero:

$$B_{\mathrm{MNa}} + 2B_{\mathrm{MCa}} + 2B_{\mathrm{M_2Ca}} - n^{\mathrm{tot}}\theta_{\mathrm{n}} + \theta_{\mathrm{s}} \left(C_{\mathrm{Na}} + 2C_{\mathrm{Ca}} - C_{\mathrm{Cl}}\right) = 0. \tag{10}$$

Force balance equations (11)-(12) for the two-phase gel, along with the incompressibility condition (2), are solved to determine the velocities of the two phases and the pressure, p. The network and solvent viscosities are η_{n} and η_{s}, respectively, while ξ/ν_{n} is the drag coefficient for relative motion between the solvent and network. (ν_{n} is defined below.)

$$\nabla \cdot \left(\theta_{\mathrm{n}} \underline{\underline{\sigma}}^{\mathrm{n}}(\mathbf{u}_{\mathrm{n}})\right) - \frac{\xi}{\nu_{\mathrm{n}}} \theta_{\mathrm{n}}\theta_{\mathrm{s}} \left(\mathbf{u}_{\mathrm{n}} - \mathbf{u}_{\mathrm{s}}\right) - \theta_{\mathrm{n}} \nabla p + \mathbf{f}_{\mathrm{n}}^{\mathrm{E}} + \mathbf{f}_{\mathrm{n}}^{\mathrm{I}} + \mathbf{f}_{\mathrm{n}}^{\mathrm{S}} = 0, \tag{11}$$

$$\nabla \cdot \left(\theta_{\mathrm{s}} \underline{\underline{\sigma}}^{\mathrm{s}}(\mathbf{u}_{\mathrm{s}})\right) - \frac{\xi}{\nu_{\mathrm{n}}} \theta_{\mathrm{n}}\theta_{\mathrm{s}} \left(\mathbf{u}_{\mathrm{s}} - \mathbf{u}_{\mathrm{n}}\right) - \theta_{\mathrm{s}} \nabla p + \mathbf{f}_{\mathrm{s}}^{\mathrm{E}} + \mathbf{f}_{\mathrm{s}}^{\mathrm{I}} + \mathbf{f}_{\mathrm{s}}^{\mathrm{S}} = 0. \tag{12}$$

The viscous stress tensors in (11)-(12) are given by

$$\underline{\underline{\sigma}}^{\mathrm{i}} = \eta_{\mathrm{i}} \left(\nabla \mathbf{u}_{\mathrm{i}} + (\nabla \mathbf{u}_{\mathrm{i}})^{\mathbf{T}}\right) - (\eta_{\mathrm{i}} \nabla \cdot \mathbf{u}_{\mathrm{i}}) \underline{\underline{I}} \qquad \mathrm{i} = \mathrm{n}, \mathrm{s}. \tag{13}$$

We solve the model equations (1)-(12) numerically using the schemes described in detail in [10].

The charged nature of the ionic species induces an electric potential that exerts forces on the charged entities present in the gel. The long-range electric force densities on the network and solvent, respectively, are

$$\mathbf{f}_{\mathrm{n}}^{\mathrm{E}} = -\frac{\theta_{\mathrm{n}}}{\nu_{\mathrm{n}}} \frac{B_{\mathrm{MNa}} + 2B_{\mathrm{MCa}} + 2B_{\mathrm{M_2Ca}} - n^{\mathrm{tot}}\theta_{\mathrm{n}}}{n^{\mathrm{tot}}\theta_{\mathrm{n}}} k_B T \nabla \Psi, \tag{14}$$

$$\mathbf{f}_{\mathrm{s}}^{\mathrm{E}} = -\frac{\theta_{\mathrm{s}}}{\nu_{\mathrm{s}}} \frac{C_{\mathrm{Na}} + 2C_{\mathrm{Ca}} - C_{\mathrm{Cl}}}{s^{\mathrm{tot}}} k_B T \nabla \Psi. \tag{15}$$

Here, ν_{n} and ν_{s} are the volume of individual network and solvent molecules, respectively, while the molar concentrations of these particles in pure network and pure solvent are n^{tot} and s^{tot} (related by $\nu_{\mathrm{n}} n^{\mathrm{tot}} = \nu_{\mathrm{s}} s^{\mathrm{tot}}$). The entropic force densities on the network and solvent are

$$\mathbf{f}_{\mathrm{n}}^{\mathrm{S}} = -\frac{k_B T}{\nu_n} \left(\frac{1}{N_{\mathrm{chain}}} + \left(1 - \frac{1}{N_{\mathrm{chain}}}\right) \theta_{\mathrm{n}}\right) \nabla \theta_{\mathrm{n}}, \tag{16}$$

$$\mathbf{f}_{\mathrm{s}}^{\mathrm{S}} = -\frac{k_B T}{\nu_{\mathrm{n}}} \left(\left(\frac{1}{N_{\mathrm{chain}}} - 1\right) \theta_{\mathrm{s}} \nabla \theta_{\mathrm{s}} + \nabla \theta_{\mathrm{s}}\right). \tag{17}$$

The short-range interaction force densities on the network and solvent are

$$\mathbf{f}_{\mathrm{n}}^{\mathrm{I}} = -\frac{k_B T \theta_{\mathrm{n}}}{\nu_{\mathrm{n}}} \nabla \left(\frac{i(\alpha)}{2} {\theta_{\mathrm{s}}}^2 + \mu_{\mathrm{n}}^0(\alpha)\right), \tag{18}$$

ICCS Camera Ready Version 2023
To cite this paper please use the final published version:
DOI: 10.1007/978-3-031-36030-5_27

$$\mathbf{f}_{\mathrm{s}}^{\mathrm{I}} = -\frac{k_B T \theta_{\mathrm{s}}}{\nu_{\mathrm{n}}} \nabla \left(\frac{i(\alpha)}{2} {\theta_{\mathrm{n}}}^2 + \mu_{\mathrm{s}}^0 \right), \tag{19}$$

where

$$\alpha = \frac{2B_{\mathrm{M_2Ca}}}{n^{\mathrm{tot}} \theta_{\mathrm{n}}}, \tag{20}$$

$$i(\alpha) = z(2\epsilon_{\mathrm{us}} - \epsilon_{\mathrm{uu}} - \epsilon_{\mathrm{ss}}) - 2\left(1 - \frac{1}{N_{\mathrm{chain}}}\right)(\epsilon_{\mathrm{us}} - \epsilon_{\mathrm{uu}}) - (\epsilon_{\mathrm{us}} - \epsilon_{\mathrm{uu}})\alpha, \tag{21}$$

$$\mu_{\mathrm{n}}^0(\alpha) = \epsilon_{\mathrm{uu}} \frac{z}{2} + (\epsilon_{\mathrm{pp}} - \epsilon_{\mathrm{uu}}) \left(1 - \frac{1}{N_{\mathrm{chain}}}\right) + \frac{\alpha}{2}(\epsilon_{\mathrm{xx}} - \epsilon_{\mathrm{uu}}). \tag{22}$$

and

$$\mu_{\mathrm{s}}^0 = \epsilon_{\mathrm{ss}} \frac{z}{2}. \tag{23}$$

Here, α is the fraction of monomers crosslinked by doubly bound calcium ions, μ_{n}^0 and μ_{s}^0 are the standard free energies of pure network and pure solvent, and $i(\alpha)$ corresponds to the interaction parameter from Flory-Huggins mixture theory [7]. This quantity may be thought of as the change in chemical energy due to mixing. Through its dependence on α, $i(\alpha)$ changes as crosslinks are formed and broken, which represents a major novelty of this model framework.

The expressions for $i(\alpha)$, $\mu_{\mathrm{n}}^0(\alpha)$, and μ_{s}^0 are derived using lattice-based mean-field arguments [8]. In these expressions, "interaction energies" represent the energy associated with various particles occupying adjacent locations on the lattice. The energies are ϵ_{xx} and ϵ_{uu} for adjacent crosslinked and uncrosslinked network particles from different polymer chains, ϵ_{pp} for adjacent particles in the same chain, ϵ_{ss} for adjacent solvent particles, and ϵ_{us} for adjacent network and solvent particles.

Of the three chemical forces acting on the gel, the entropic force always promotes swelling/mixing and the electric force tends to resist the relative motion between the network and the solvent [10]. Therefore, in the experiments below, the deswelling/collapsing of a gel is driven by the short range interaction force. Based on Eqs. (18)-(19) and ignoring the terms that are constant in space (μ_{s}^0 and the first two terms in $\mu_{\mathrm{n}}^0(\alpha)$), we may rewrite the short range forces as:

$$\mathbf{f}_{\mathrm{n}}^{\mathrm{I}} = \frac{k_B T \theta_{\mathrm{n}}}{\nu_{\mathrm{n}}} \left(\frac{\theta_{\mathrm{s}}^2 \epsilon_1 - \epsilon_3}{2} \nabla\alpha - i(\alpha)\theta_{\mathrm{s}} \nabla\theta_{\mathrm{s}} \right) = \mathbf{f}_{\mathrm{n}}^{\mathrm{I},1} + \mathbf{f}_{\mathrm{n}}^{\mathrm{I},2} + \mathbf{f}_{\mathrm{n}}^{\mathrm{I},3}, \tag{24}$$

$$\mathbf{f}_{\mathrm{s}}^{\mathrm{I}} = \frac{k_B T \theta_{\mathrm{s}}}{\nu_{\mathrm{n}}} \left(\frac{\theta_{\mathrm{n}}^2}{2} \epsilon_1 \nabla\alpha - i(\alpha)\theta_{\mathrm{n}} \nabla\theta_{\mathrm{n}} \right) = \mathbf{f}_{\mathrm{s}}^{\mathrm{I},1} + \mathbf{f}_{\mathrm{s}}^{\mathrm{I},2}. \tag{25}$$

Here $\epsilon_1 = \epsilon_{\mathrm{us}} - \epsilon_{\mathrm{uu}}$. In this work, we assume $\epsilon_1 < 0$, which implies an uncrosslinked, network monomer "prefers" to be adjacent to a solvent particle rather than to another negatively charged monomer. Similarly, we assume $\epsilon_3 = \epsilon_{\mathrm{xx}} - \epsilon_{\mathrm{uu}} < 0$, and thus the interaction energy between network monomers is reduced by calcium crosslinking. To facilitate later discussion, we have partitioned $\mathbf{f}_{\mathrm{n}}^{\mathrm{I}}$ and $\mathbf{f}_{\mathrm{s}}^{\mathrm{I}}$ into components:

$$\mathbf{f}_{\mathrm{n}}^{\mathrm{I},1} = \frac{k_B T \theta_{\mathrm{n}} \theta_{\mathrm{s}}^2}{2\nu_{\mathrm{n}}} \epsilon_1 \nabla\alpha, \quad \mathbf{f}_{\mathrm{n}}^{\mathrm{I},2} = -\frac{k_B T \theta_{\mathrm{n}} \theta_{\mathrm{s}}}{\nu_{\mathrm{n}}} i(\alpha) \nabla\theta_{\mathrm{s}}, \quad \text{and} \quad \mathbf{f}_{\mathrm{n}}^{\mathrm{I},3} = -\frac{k_B T \theta_{\mathrm{n}}}{2\nu_{\mathrm{n}}} \epsilon_3 \nabla\alpha.$$

ICCS Camera Ready Version 2023
To cite this paper please use the final published version:
DOI: 10.1007/978-3-031-36030-5_27

$$\mathbf{f}_{\mathrm{s}}^{\mathrm{I},1} = \frac{k_B T \theta_{\mathrm{s}} \theta_{\mathrm{n}}^2}{2\nu_{\mathrm{n}}} \epsilon_1 \nabla \alpha \quad \text{and} \quad \mathbf{f}_{\mathrm{s}}^{\mathrm{I},2} = -\frac{k_B T \theta_{\mathrm{s}} \theta_{\mathrm{n}}}{\nu_{\mathrm{n}}} i(\alpha) \nabla \theta_{\mathrm{n}}.$$

Note that $\mathbf{f}_{\mathrm{n}}^{\mathrm{I},2} = -\mathbf{f}_{\mathrm{s}}^{\mathrm{I},2}$. These forces are completely analogous to classical Flory-Huggins polymer theory. They tend to drive swelling/mixing when $i(\alpha) < 0$ and to drive deswelling when $i(\alpha) > 0$. Both $\mathbf{f}_{\mathrm{n}}^{\mathrm{I},1}$ and $\mathbf{f}_{\mathrm{s}}^{\mathrm{I},1}$ are novel to this model (they do not have analogs in Flory-Huggins theory). Both are oriented in the direction of decreasing α, driving material towards a spatial location with a lower crosslink fraction α. For a low-density network ($\theta_{\mathrm{n}} \ll 1$), $\mathbf{f}_{\mathrm{n}}^{\mathrm{I},1}$ is much larger in magnitude than $\mathbf{f}_{\mathrm{s}}^{\mathrm{I},1}$. Finally, $\mathbf{f}_{\mathrm{n}}^{\mathrm{I},3}$ tends to drive the network towards a region with higher α. Therefore, the forces on the network $\mathbf{f}_{\mathrm{n}}^{\mathrm{I},1}$ and $\mathbf{f}_{\mathrm{n}}^{\mathrm{I},3}$ play opposite roles for the same spatial distribution of α. For $\theta_{\mathrm{s}} \approx 1$, the direction of $\mathbf{f}_{\mathrm{n}}^{\mathrm{I},1} + \mathbf{f}_{\mathrm{n}}^{\mathrm{I},3}$ is determined by the relative magnitudes of ϵ_1 and ϵ_3 (i.e. is the energy of the lattice reduced more by replacing monomer/monomer interactions with monomer/solvent interactions or by crosslinks) . As shown in our results section, depending on the relative magnitude of the interaction energies, the ion-induced volume transition in gels may exhibit drastically different patterns.

3 Simulation Results

3.1 Model Parameters and Problem Setup

The values of model parameters, similar to those used in [9, 10], are listed in Table 1. We choose the values of the interaction energies so that the interaction parameter $i(\alpha)$ in Eq. (21) is $i(\alpha) = 18\alpha - 2.76$, an increasing linear function of α. As the value of α increases from 0 to 1, $i(\alpha)$ changes from negative to positive so that the roles of the classical Flory-Huggins terms $\mathbf{f}_{\mathrm{n}}^{\mathrm{I},2}$ and $\mathbf{f}_{\mathrm{s}}^{\mathrm{I},2}$ switch from promoting swelling (mixing of the phases) to promoting deswelling (phase separation). The ion binding and unbinding rate coefficients in the table imply that calcium has a smaller dissociation constant, so calcium binding to the network is chemically preferred. The computational domain is a 2D square of size 20 μm $\times$ 20 μm. Both velocities are assumed to be zero along its boundaries. No flux boundary conditions are applied to each dissolved ion concentration on all boundaries. A computational grid of size 256 $\times$ 256 is used for all simulations. The time step is fixed at $\Delta \mathrm{t} = 2.0 \times 10^{-7}$s. The typical distribution of the model variables at the initial time is shown in Fig. 1. The initial profiles of the network volume fraction and bound ion distributions are set to represent a blob of gel with loosely packed network ($\theta_{\mathrm{n}} \approx 5\%$), immersed in a fluid solvent with a high concentration of divalent calcium ions. The region with an appreciable amount of network is referred to as the "gel"; the rest of the domain is referred to as the "bath". This setup mimics the experiments in [12]. Spatially constant concentrations of dissolved ions with zero net charge are set in the bath, with the concentration of calcium much higher than that of sodium. We denote initial bath concentrations of ions with the asterisk superscript: C_i^*. The initial conditions for the ion concentrations in the gel region are chosen so that the binding and unbinding reactions are in local chemical equilibrium [10].

ICCS Camera Ready Version 2023
To cite this paper please use the final published version:
DOI: 10.1007/978-3-031-36030-5_27

parameter	value
network viscosity $\eta_{\rm n}$	100 Poise
solvent viscosity $\eta_{\rm s}$	0.01 Poise
diffusion coefficient $D_{\rm j}$	2.5×10^{-5} cm^2/s
drag coefficient ξ/ν	2.5×10^{9} g/(cm^{3}s)
$\epsilon_{\rm us} - \epsilon_{\rm uu}$ (ϵ_1)	-18.0
$\epsilon_{\rm us} - \epsilon_{\rm ss}$	11.6
$\epsilon_{\rm xx} - \epsilon_{\rm uu}$ (ϵ_3)	variable
$\epsilon_{\rm pp} - \epsilon_{\rm uu}$	0
number of monomers in a chain N	100
network charge density $n^{\rm tot}$	0.1 Molar
size of monomer $\nu_{\rm n}$	1.661×10^{-8} μm^3
coordination number z	6
ion valences $z_{\rm Na}$, $z_{\rm Ca}$, $z_{\rm Cl}$	1, 2, -1
$k^{\rm on}_{\rm Ca}$	5×10^{6} M^{-1}s^{-1}
$k^{\rm off}_{\rm Ca}$	5×10^{2} M^{-1}s^{-1}
$k^{\rm on}_{\rm Na}$	10^{6} M^{-1}s^{-1}
$k^{\rm off}_{\rm Na}$	10^{3} M^{-1}s^{-1}

Table 1: Simulation parameters.

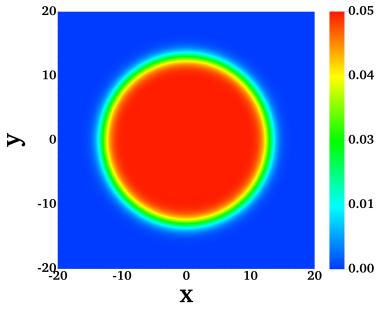

(a) Initial distribution of $\theta_{\rm n}$.

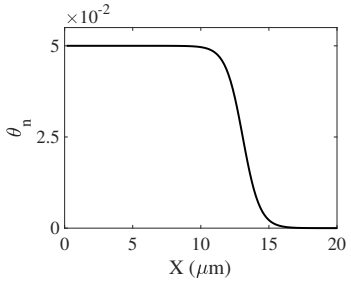

(b) Profile of $\theta_{\rm n}$ at $t = 0$ along the positive x-axis.

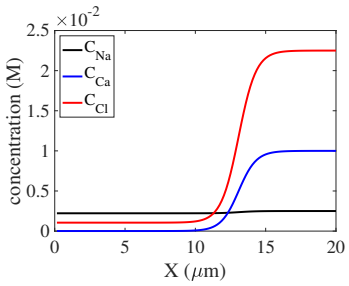

(c) Profiles of the concentrations for dissolved ions at $t = 0$ along the positive x-axis.

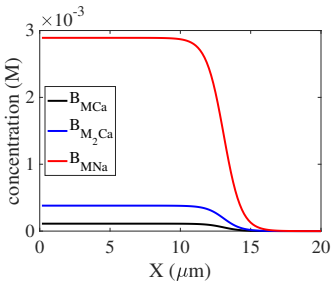

(d) Profiles of the concentrations of bound ions at $t = 0$ along the positive x-axis.

Fig. 1: The 2D computational domain and initial distributions of model variables.

ICCS Camera Ready Version 2023
To cite this paper please use the final published version:
DOI: 10.1007/978-3-031-36030-5_27

For the initial profiles shown in Fig. 1, we have $\alpha \approx 0.153$ and the interaction parameter i is approximately zero. The spatially uniform profiles in the gel and in the bath are connected smoothly through a hyperbolic tangent function.

3.2 Effect of calcium bath concentration on gel deswelling

To investigate the effect of calcium ion concentration in the bath, we carried out two simulations with $C^*_{\mathrm{Ca}} = 0.001$ M and $C^*_{\mathrm{Ca}} = 0.01$ M, respectively. The bath sodium concentration is fixed at a relatively low value of $C^*_{\mathrm{Na}} = 0.0025$ M.

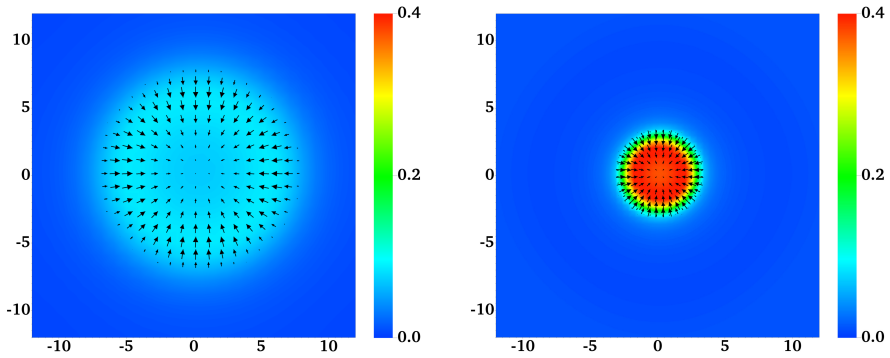

(a) $||\mathbf{u}_{\mathrm{n}}||^{\max} = 0.21$ mm/s. (b) $||\mathbf{u}_{\mathrm{n}}||^{\max} = 0.32$ mm/s.

Fig. 2: The distribution of θ_{n} and $\mathbf{u}_{\mathrm{n}}$ at t = 5.6 ms for (a) $C^*_{\mathrm{Ca}} = 0.001$ M and (b) $C^*_{\mathrm{Ca}} = 0.01$ M. $\epsilon_3 = -0.1$. The vectors have different scales.

In this subsection, $\epsilon_3 = -0.1$ so that crosslinks only slightly reduce the interaction energy between monomers. At the start of these simulations, the crosslink fraction α is higher near the edge of the gel abutting the bath where the calcium concentration is higher than in the gel's interior. As a consequence, $i(\alpha)$ is positive there, favoring deswelling. The distributions of θ_{n} and $\mathbf{u}_{\mathrm{n}}$ at t = 5.6 ms are plotted in Fig. 2. We see that as the network moves inward towards the center of the domain, the gel becomes smaller and more dense relative to its initial profile. We refer to this behavior as "collapse". A greater collapse is observed for higher C^*_{Ca}. In both simulations, the maximum magnitude of $\mathbf{u}_{\mathrm{n}}$ decreases with time (not shown). Plots of C_{Ca} and $\mathbf{u}_{\mathrm{s}}$ at the same time are shown in Fig. 3. In contrast to the network velocity, the solvent velocity exhibits complicated patterns. With the inward movement of the network, the solvent moves outward from the center of the gel. The solvent velocity near the gel's center is much larger with the higher bath calcium concentration. Due to diffusion, the distribution of C_{Ca} becomes more homogeneous with time (not shown).

ICCS Camera Ready Version 2023
To cite this paper please use the final published version:
DOI: 10.1007/978-3-031-36030-5_27

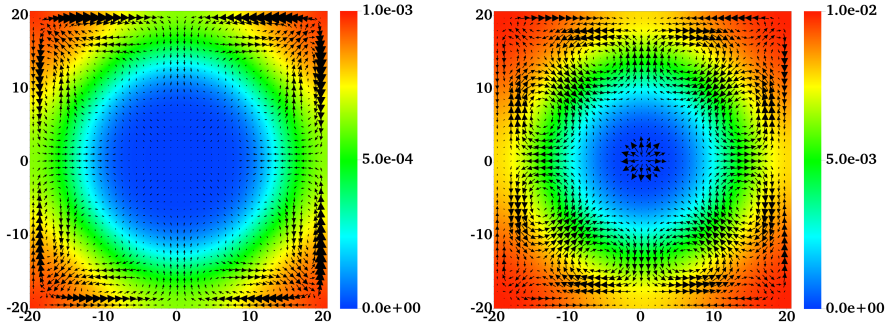

(a) $||\mathbf{u}_s||^{max} = 0.33$ mm/s. (b) $||\mathbf{u}_s||^{max} = 0.21$ mm/s.

Fig. 3: The distribution of C_{Ca} and $\mathbf{u}_s$ at t = 5.6 ms for (a) $C^*_{Ca} = 0.001$ M and (b) $C^*_{Ca} = 0.01$ M. $\epsilon_3 = -0.1$. All vectors have the same scale.

In Fig. 4, we plot the distributions of θ_n and α along the positive x-axis. Relative to its initial profile, the distribution of θ_n becomes more inhomogeneous with the development of large peak values close to the gel's center. There is a more profound collapse in the simulation with a higher bath calcium concentration. As shown in Figs. 4ab, as the value of C^*_{Ca} changes from 0.001 M to 0.01 M, the peak of α increases greatly. Notice that for both simulations, α is larger than its initial value of 0.153 over the large portions of the gel with significant network volume fractions. The interaction parameter $i(\alpha)$ is positive in those regions, and so the short range force components $\mathbf{f}_n^{I,2}$ and $\mathbf{f}_s^{I,2}$ both promote deswelling. Because $|\epsilon_3| \ll |\epsilon_1|$, $|\mathbf{f}_n^{I,3}| \ll |\mathbf{f}_n^{I,1}|$, and therefore $\mathbf{f}_n^{I,3}$ does not appreciably deter collapse.

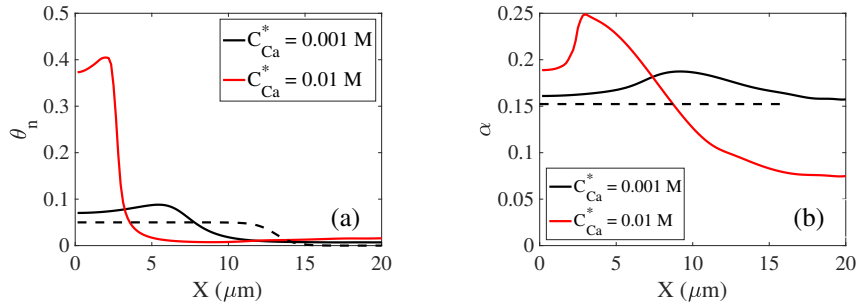

Fig. 4: 1D distributions of (a) θ_n and (b) α at t = 5.6 ms for $C^*_{Ca} = 0.001$ M and 0.01 M. $\epsilon_3 = -0.1$. The dashed lines show the corresponding initial profiles.

ICCS Camera Ready Version 2023
To cite this paper please use the final published version:
DOI: 10.1007/978-3-031-36030-5_27

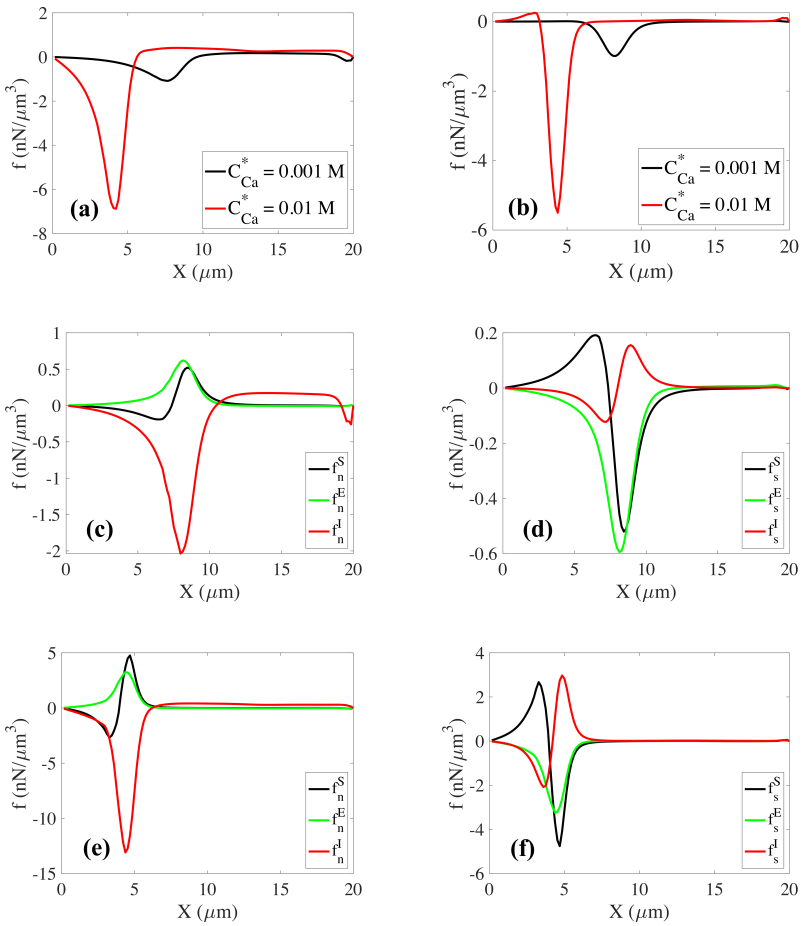

Fig. 5: Force densities along the positive **x**-axis at t = 2.8 ms. Total chemical force densities on (a) network and (b) solvent. Components of the chemical force densities for $C^*_{\mathrm{Ca}} = 0.001$ M on (c) network and (d) solvent. Components of the chemical force densities for $C^*_{\mathrm{Ca}} = 0.01$ M on (e) network and (f) solvent.

To understand the roles played by different chemical forces in deswelling, we plot their 1D distributions at t = 2.8 ms in Fig. 5. Figs. 5ab show that the total chemical forces on both the network and the solvent are directed towards the center of the gel and that the magnitude of the forces is much larger for the higher bath calcium concentration. A detailed look at the plots Figs. 5c-f indicates that: (1) The electric forces (green solid lines) on the network and on the solvent resist gel deswelling. The magnitude of the electric force increases with C^*_{Ca}, consistent with our previous study [9]. (2) From the center to the edge, the entropic force (black solid lines) changes direction and tends to homogenize

ICCS Camera Ready Version 2023
To cite this paper please use the final published version:
DOI: 10.1007/978-3-031-36030-5_27

the distribution of θ_n and θ_s. (3) The short range forces (red solid curves in c and e) mainly drive the network towards the center, promoting gel deswelling. Since α has a sharper gradient in the simulation with $C^*_{Ca} = 0.01$ M, the corresponding short range force is also much larger. The location where $\mathbf{f}^I_n$ changes direction is consistent with the location where α is highest (plot not shown). On the other hand, $\mathbf{f}^I_s$ (red solid curves in d and f) also changes direction, at locations different from that for $\mathbf{f}^I_n$.

3.3 Effect of Interaction Parameter

Next, we report on two simulations with $\epsilon_3 = -10$ and $\epsilon_3 = -18$. The purpose is to study parameter regimes in which crosslink formation can cause a substantial drop in interactive energy between monomers (relative to monomer/solvent mixing). The bath calcium concentration is $C^*_{Ca} = 0.01$ M. All other parameters are identical to those of the simulations shown in section 3.2. As the value ϵ_3 gets more negative (with $|\epsilon_3| \leq |\epsilon_1|$), the magnitude of network force component $\mathbf{f}^{I,3}_n$ increases. With other conditions being the same, this tends to decrease the magnitude of the combined force $\mathbf{f}^{I,1}_n + \mathbf{f}^{I,3}_n$ and contributes to there being less deswelling.

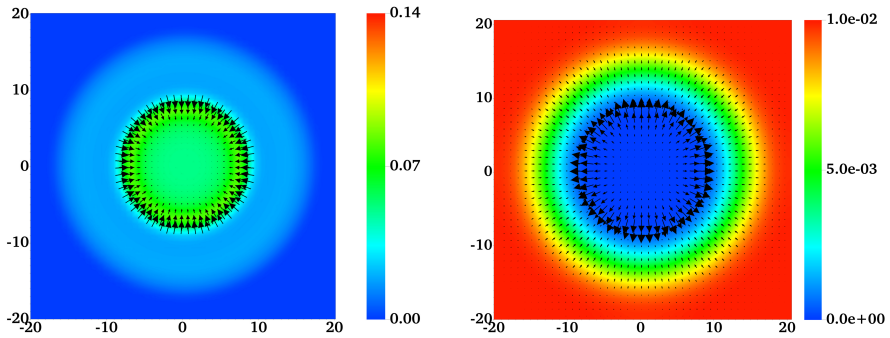

(a) $||\mathbf{u}_n||^{max} = 0.59$ mm/s. (b) $||\mathbf{u}_s||^{max} = 0.43$ mm/s.

Fig. 6: The distribution of θ_n and $\mathbf{u}_n$ (a) and C_{Ca} and $\mathbf{u}_s$ (b) at t = 1.6 ms for $\epsilon_3 = -10$. The vectors have different scales.

For the simulation with $\epsilon_3 = -10$, the solvent tends to flow outwards, away from the gel center as the network collapses inward, similar to the previous section. The distributions of θ_n, $\mathbf{u}_n$, C_{Ca} and $\mathbf{u}_s$ at t = 1.6 ms are plotted in Fig. 6. Comparison between Fig. 6a and the results at the same time from the simulations of the previous section (not shown) indicates that the extent of deswelling is greatly reduced as the value of ϵ_3 is changed from -0.1 to -10.

As the value of ϵ_3 is further reduced to -18, network accumulation is observed along the edge of the gel and a ring pattern is formed (see Fig. 7). Concurrently, solvent is depleted from the edge of the gel, where the high density network

ICCS Camera Ready Version 2023
To cite this paper please use the final published version:
DOI: 10.1007/978-3-031-36030-5_27

ring is formed. Solvent thus moves from this region both toward the origin and toward the domain boundary.

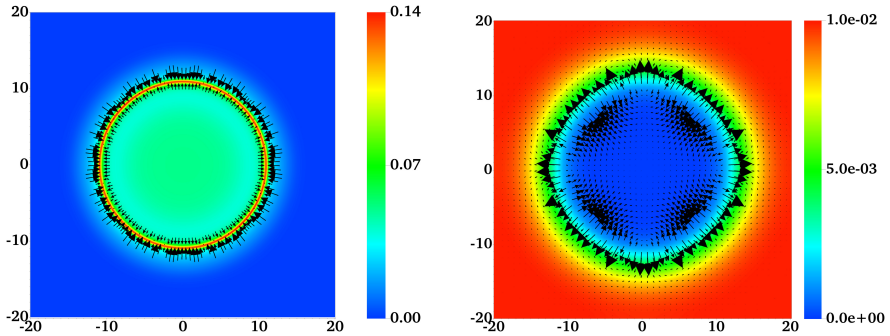

(a) $||\mathbf{u}_\mathrm{n}||^{\max} = 0.12$ mm/s. (b) $||\mathbf{u}_\mathrm{s}||^{\max} = 0.1$ mm/s.

Fig. 7: The distribution of θ_n and $\mathbf{u}_\mathrm{n}$ (a) and C_Ca and $\mathbf{u}_\mathrm{s}$ (b) at t = 1.6 ms for $\epsilon_3 = -18$. The vectors have different scales.

Fig. 8 shows the 1D distributions of θ_n and α at t = 1.6 ms. When $\epsilon_3 = -18$, these quantities become strikingly inhomogeneous, with greater θ_n and α accumulation near the edge of the gel. There is very little movement of the network towards the origin when, indicated by the locations of the peak values of θ_n and α. Since α is large in a portion of the gel near its edge, $i(\alpha)$ is positive in those regions so that the short range force components $\mathbf{f}_\mathrm{n}^{\mathrm{I},2}$ and $\mathbf{f}_\mathrm{s}^{\mathrm{I},2}$ (not shown) drive more network into the ring and expel solvent from it. In the regions away from the edge of the gel where $i(\alpha)$ is negative, $\mathbf{f}_\mathrm{n}^{\mathrm{I},2}$ and $\mathbf{f}_\mathrm{s}^{\mathrm{I},2}$ promote solvent/network mixing.

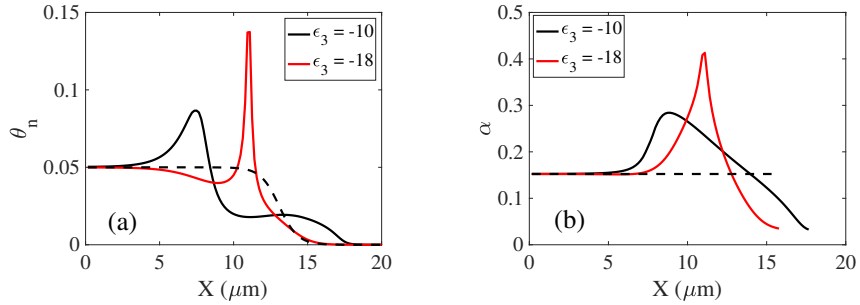

Fig. 8: 1D distributions of (a) θ_n and (b) α at t = 1.6 ms for $\epsilon_3 = -10$ and $\epsilon_3 = -18$. The black dashed lines show the initial profiles.

To further elucidate the ring formation seen for $\epsilon_3 = -18$ (and compare with the collapse seen for $\epsilon_3 = -10$), the 1D distributions of the chemical force densities at t = 0.8 ms are plotted in Fig. 9. Fig. 9a shows that the total chemical

ICCS Camera Ready Version 2023
To cite this paper please use the final published version:
DOI: 10.1007/978-3-031-36030-5_27

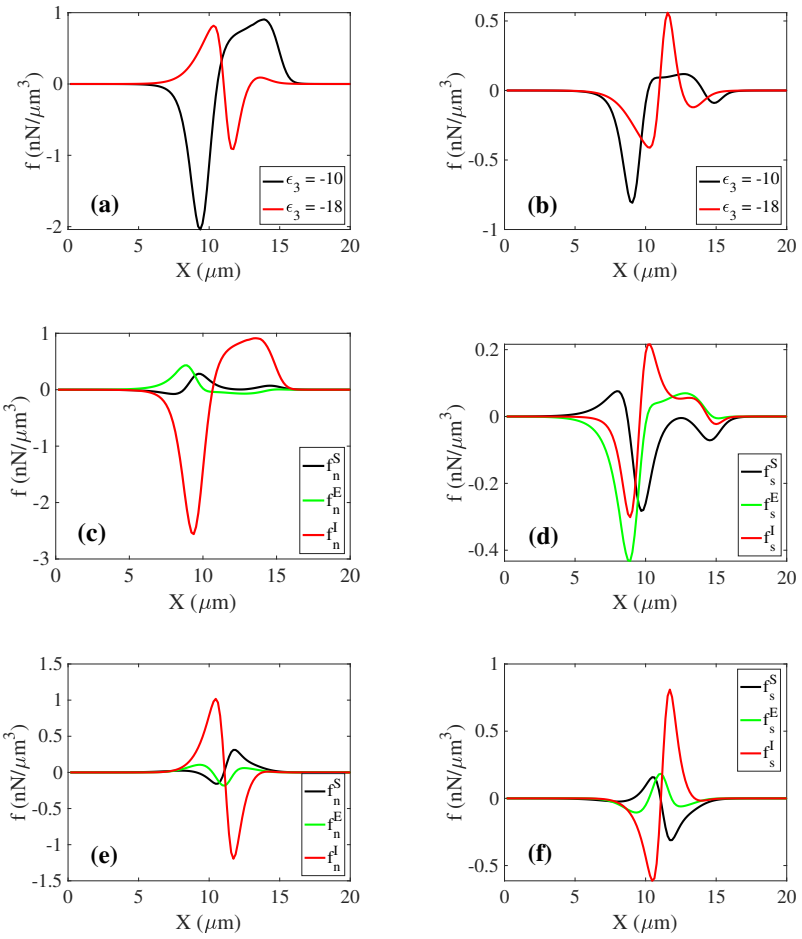

Fig. 9: 1D force density distributions at t = 0.8 ms for $\epsilon_3 = -10$ and -18. Total chemical force density in (a) network and (b) solvent. For $\epsilon_3 = -10$, components of chemical force density on (c) network and (d) solvent. For $\epsilon_3 = -18$, components of chemical force density on (e) network and (f) solvent.

force on the network is directed toward the edge of the gel (from both directions) when $\epsilon_3 = -18$, while the force is directed towards the center of the gel for $\epsilon_3 = -10$. For $\epsilon_3 = -18$, the force over the region where the network is being driven "outwards" is nearly equal in magnitude to the force over the region where the network is being driven "inwards". These opposing forces result in the ring formation observed in Fig. 7. At t = 0.8 ms the total chemical force on the solvent is directed away from the edge of the gel, in both directions, as shown in Fig. 9b. A detailed look at the plots c-f indicates that: (1) The electric

ICCS Camera Ready Version 2023
To cite this paper please use the final published version:
DOI: 10.1007/978-3-031-36030-5_27

forces (green solid lines) on the network and solvent are equal in magnitude with opposite directions. For $\epsilon_3 = -10$, the electric force resists deswelling by driving the network towards the edge of the gel and the solvent towards the center. For $\epsilon_3 = -18$, the electric force resists ring formation by driving the network away from the edge and the solvent towards the edge so the two phases can mix. (2) The entropic force tends to homogenize the distribution of θ_n (and θ_s) as indicated by the changing direction of the entropic forces (black solid lines). (3) The short range force for $\epsilon_3 = -10$ in (c) drives the network towards the center, leading to collapse. A detailed look at the individual components of the short range force for $\epsilon_3 = -18$ (plot not shown) indicates that $\mathbf{f}_n^{I,1}$ and $\mathbf{f}_n^{I,3}$ exert a nearly equal and opposite force on the network, leaving $\mathbf{f}_n^{I,2}$ to dominate. Since $i(\alpha)$ is positive over some portion of the gel and negative over another because of how α is distributed (see Fig. 8b), then $\mathbf{f}_n^{I,2}$ causes deswelling over the region where $i(\alpha) < 0$ and causes swelling over the region where $i(\alpha) > 0$. The location where $\mathbf{f}_n^{I}$ changes direction is consistent with the location where α takes its maximum in Fig. 8b. As a result, we observe accumulation of the network near the edge of the gel.

4 Conclusion

Our computational studies reveal multiple qualitatively distinct forms of deswelling which may be exhibited by a model of polyelectrolyte gel. In particular, we show that the bath ionic composition and relative magnitudes of the interaction energies play a significant role in determining the deswelling dynamics of the gel. Specifically, our results indicate that different components of the short range interaction force can drive swelling *or* deswelling of the gel. In the case where $|\epsilon_3| \ll |\epsilon_1|$, the dominant components of the short-range interaction forces drive the gel to collapse. As $|\epsilon_3|$ increases to roughly the same scale as $|\epsilon_1|$, the gel collapse is reduced significantly due to the greater competition between different component of the interaction force. It is worth noting that this form of gel collapse, and its dependence on the ionic composition of the bath has been studied in numerous theoretical and experimental systems, and is a widespread behavior of polyelectrolyte gel systems [13]. Finally, for $|\epsilon_3| = |\epsilon_1|$ we observe a more complex behavior characterized by network accumulation near the gel's edge, resulting in a ring pattern. In this case the Flory-Huggins interaction parameter, $i(\alpha)$, plays a dominant role in determining the dynamics of the gel, becoming positive as the network forms crosslinks and leading to the formation of network ring. Similar roles played by the Flory-Huggins interaction parameter were reported in experimental studies [12]. Pattern formation during gel deswelling (sometimes called spinodal decomposition) has been observed in other model systems and other geometries [14], though to our knowledge this work represents the first time it has been reported in a model which incorporates a crosslink-dependent interaction energy. Our computational results from varying the interactive energies between network and solvent particles motivate further investigation into behavior of gels with different properties.

ICCS Camera Ready Version 2023
To cite this paper please use the final published version:
DOI: 10.1007/978-3-031-36030-5_27

References

1. Tongu, C., Kenmotsu, T., Yoshikawa, Y., Zinchenko, A., Chen, N., Yoshikawa, K.: Divalent cation shrinks DNA but inhibits its compaction with trivalent cation. J. Chem. Phys. **144**(20), 205101 (2016)
2. Verdugo, P.: Supramolecular dynamics of mucus. Cold Spring Harb Perspect Med. **2**(11), a009597 (2012)
3. Mussel, M., Basser, P.J., Horkay, F.: Ion-induced volume transition in gels and its role in biology. Gels **7**(1), (2021)
4. Flory, P., J. Rehner, J.: Statistical mechanics of cross-linked polymer networks II. Swelling. J. Chem. Phys. **11**, 521–526 (1943)
5. Yamaue, T., Taniguchi, T., Doi, M.: Shrinking process of gels by stress-diffusion coupled dynamics. Theor. Phys. Supp. **138**, 4160–417 (2000)
6. Zhang, H., Dehghany, M., Hu, Y.: Kinetics of polyelectrolyte gels. J. Appl. Mech. **87**(6), (2020)
7. Doi, M.: Introduction to polymer physics. Oxford University Press (1996)
8. Sircar, S., Keener, J., Fogelson, A.: The effect of divalent vs. monovalent ions on the swelling of mucin-like polyelectrolyte gels: Governing equations and equilibrium analysis. J. Chem. Phys. **138**, 014901 (2013)
9. Du, J., Lewis, O., Keener, J., Fogelson, A.: Modeling and simulation of the ion-binding-mediated swelling dynamics of mucin-like polyelectrolyte gels. Gels **7**(4), (2021)
10. Du, J., Nagda, B., Lewis, O., Szyld, D., Fogelson, A.: A computational frame-work for the swelling dynamics of mucin-like polyelectrolyte gels. J. Non-Newton. Fluid Mech. **313**, 104989 (2023)
11. Lewis, O., Keener, J., Fogelson, A.: Electrodiffusion-mediated swelling of a two-phase gel model of gastric mucus. Gels **4**(3), 76 (2018)
12. Mussel, M., Lewis, O., Basser, P.J., Horkay, F.: Dynamic model of monovalent-divalent cation exchange in polyelectrolyte gels. Phys. Rev. Mater. **6**, 035602 (2022)
13. Horkay, F., Tasaki, I., Basser, P.: Effect of monovalent-divalent cation exchange on the swelling of polyacrylate hydrogels in physiological salt solutions. Biomacromolecules **2**(1), 195–199 (2001)
14. Celora, G.L., Hennessy, M.G., Münch, A., Wagner, B., Waters, S.L.: The dynamics of a collapsing polyelectrolyte gel. arXiv preprint arXiv:2105.06495 (2021)

ICCS Camera Ready Version 2023
To cite this paper please use the final published version:
DOI: 10.1007/978-3-031-36030-5_27